Remote sensing of surface pressure on Mars with the Mars Express/OMEGA spectrometer: 1. Retrieval method

François Forget, Aymeric Spiga, Bastien Dolla, Sandrine Vinatier, Riccardo Melchiorri, Pierre Drossart, Aline Gendrin, Jean-Pierre Bibring, Yves Langevin, Brigitte Gondet

Remote sensing of surface pressure on Mars with the Mars Express/OMEGA spectrometer: 1. Retrieval method

François Forget,[1] Aymeric Spiga,[1] Bastien Dolla,[1] Sandrine Vinatier,[2] Riccardo Melchiorri,[2] Pierre Drossart,[2] Aline Gendrin,[3] Jean-Pierre Bibring,[3] Yves Langevin,[3] and Brigitte Gondet[3]

Received 28 November 2006; revised 6 July 2007; accepted 30 July 2007; published 30 August 2007.

[1] Observing and analyzing the variations of pressure on the surface of a planet is essential to understand the dynamics of its atmosphere. On Mars the absorption by atmospheric CO_2 of the solar light reflected on the surface allows us to measure the surface pressure by remote sensing. We use the imaging spectrometer OMEGA aboard Mars Express, which provides an excellent signal to noise ratio and the ability to produce maps of surface pressure with a resolution ranging from 400 m to a few kilometers. Surface pressure is measured by fitting spectra of the CO_2 absorption band centered at 2 μm. To process the hundreds of thousands of pixels present in each OMEGA image, we have developed a fast and accurate algorithm based on a line-by-line radiative transfer model which includes scattering and absorption by dust aerosols. In each pixel the temperature profile, the dust opacity, and the surface spectrum are carefully determined from the OMEGA data set or from other sources to maximize the accuracy of the retrieval. We estimate the 1-σ relative error to be around 7 Pa in bright regions and about 10 Pa in darker regions, with a possible systematic bias on the absolute pressure lower than 30 Pa (4%). The method is first tested by comparing an OMEGA pressure retrieval obtained over the Viking Lander 1 (VL1) landing site with in situ measurements recorded 30 years ago by the VL1 barometer. The retrievals are further validated using a surface pressure predictor which combines the VL1 pressure records with the MOLA topography and meteorological pressure gradients simulated with a General Circulation Model. A good agreement is obtained. In particular, OMEGA is able to monitor the seasonal variations of the surface pressure in Isidis Planitia. Such a tool can be applied to detect meteorological phenomena, as described by Spiga et al. (2007).

Citation: Forget, F., A. Spiga, B. Dolla, S. Vinatier, R. Melchiorri, P. Drossart, A. Gendrin, J.-P. Bibring, Y. Langevin, and B. Gondet (2007), Remote sensing of surface pressure on Mars with the Mars Express/OMEGA spectrometer: 1. Retrieval method, *J. Geophys. Res.*, *112*, E08S15, doi:10.1029/2006JE002871.

1. Introduction

[2] In meteorology, surface pressure measurements are crucial to characterize the dynamics of the atmosphere. Such measurements are usually performed in situ with barometers. They are thus very seldom on Mars. To this day, pressure records are available at only three locations thanks to the Viking Landers and the Mars Pathfinder probes. Nevertheless, these records have been used to characterize a wide range of meteorological phenomena such as baroclinic waves, tidal waves, dust devils, or the seasonal condensation of a significant part of the atmosphere in the polar regions [*Zurek et al.*, 1992]. The building of a network of surface weather stations that could measure surface pressure on Mars has been considered to be of high priority for Mars Exploration [*Haberle and Catling*, 1996] but such a complex and ambitious mission remains to be achieved.

[3] An alternative solution to in situ measurements is remote sensing from orbit. The hydrostatic component of the surface pressure (i.e., the weight of the atmospheric column above the surface) can be measured by retrieving the column mass of an atmospheric gas with known mixing ratio using its spectral absorption or emission. On Earth, such a measurement would be extremely useful for meteorological studies, and several attempts have been made. In particular, a pressure retrieval technique based on the absorption of reflected solar light in the O_2 A-band (759–771 nm) was studied by *Barton and Scott* [1986] and

[1] Laboratoire de Météorologie Dynamique, Institut Pierre-Simon Laplace, Paris, France.
[2] LESIA, Observatoire de Paris, Meudon, France.
[3] Institut d'Astrophysique Spatiale, Orsay, France.

0148-0227/07/2006JE002871

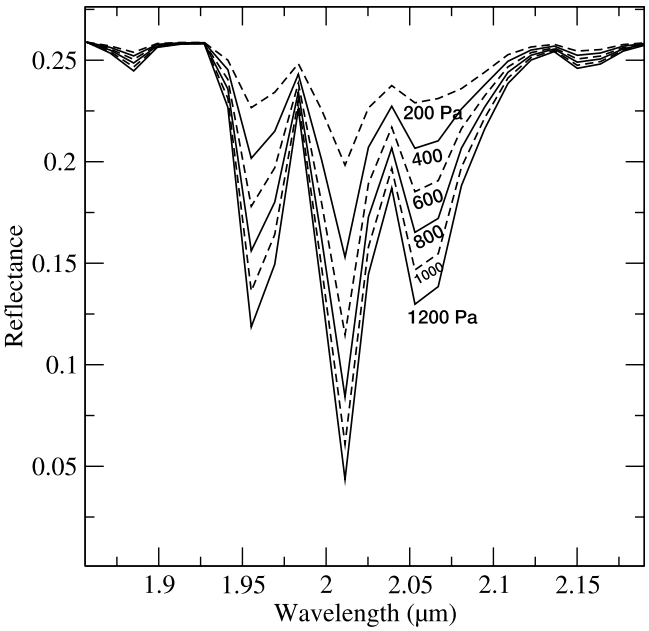

Figure 1. OMEGA-like synthetic spectra showing the strong sensitivity of the CO_2 2 μm band to surface pressure. The spectra are simulated with the same observing conditions as in a pixel containing a "ground truth" at the Viking Lander 1 site during orbit 363 (see section 4.1), which are typical of the usual observing conditions with OMEGA: solar zenith angle, 27.1°; viewing angle $\simeq$0°; dust opacity, 0.24; constant surface albedo, 0.29; temperature profile corresponding to the Viking Lander 1 site at L_s $\sim$28.2°; and local time $\sim$10.7 Martian hours.

Mitchell and O'Brien [1987], and feasibility tests from aircraft were reported by *O'Brien et al.* [1997].

[4] They found that accuracies of 0.1% could be achieved with high-resolution spectra. However, subsequent analysis of these data, and O_2 A-band observations from the Global Ozone Monitoring Experiment (GOME) spectrometer aboard ERS-2 and from the SCanning Imaging Absorption SpectroMeter for Atmospheric CartograpHY (SCIAMACHY) imaging spectrometer on the ESA ENVISAT satellite, have revealed issues with this approach, especially when applied to such high-resolution, polarization-sensitive instruments in aerosol-laden atmospheres [e.g., *Stam et al.*, 2000; *Bösch et al.*, 2006]. Nevertheless, while O_2 measurements from existing space-based instruments are not yet accurate enough for Earth meteorology, they are now being routinely used to estimate cloud-top pressures [*Dubuisson et al.*, 2001; *Fournier et al.*, 2006]. Similar studies have also been performed to measure the column mass of CO_2, a gas characterized by many absorption lines in the near-infrared. Because the CO_2 mixing ratio varies in space and time on Earth, the objective of such studies is to map the abundance of CO_2 rather than measuring surface pressure. Within that context, the feasibility and characterization of space-based CO_2 measurements from SCIAMACHY and other instruments have been extensively discussed [see, e.g., *Bösch et al.*, 2006, and references therein]. A dedicated mission, the NASA Orbiting Carbon Observatory mission (OCO) has been designed [*Crisp et al.*, 2004]. It is expected to measure the column-averaged CO_2 mixing ratio with a precision of about 0.3% on regional scales.

[5] On Mars, the atmosphere is mostly composed of carbon dioxyde. The absorption by CO_2 of the solar light reflected by the Martian surface can easily be measured, providing a good indicator of the amount of CO_2 in the atmosphere, and thus of the surface pressure. In this paper, we present a tentative study to retrieve the surface pressure on Mars as accurately as possible using the OMEGA imaging spectrometer aboard Mars Express. With such an instrument, we can produce maps of surface pressure with various resolution down to 400 m.

[6] Following the pioneering work performed from the Earth by astronomers like *Gray* [1966] and from orbital data by *Rosenqvist* [1991], *Bibring et al.* [1991], and *Gendrin et al.* [2003] with the Infrared Mapping Spectrometer (ISM) aboard the Phobos 2 spacecraft, we use the CO_2 absorption band centered at 2 μm. This band is strong enough to provide a clear signal almost proportional to surface pressure (Figure 1), but it never saturates at OMEGA resolution under Martian conditions (note that many of the individual spectral lines that compose the CO_2 spectra around 2 μm do saturate, but their combined absorption seen at OMEGA resolution does not).

[7] In this paper, we first present in details the models and the retrieval method that we have used to process the OMEGA data. We provide some estimations of the associated absolute and relative errors. Finally, we show some example of measurements of surface pressure on Mars. In a companion paper, *Spiga et al.* [2007] apply our method to map surface pressure in multiple areas on Mars and characterize various meteorological phenomena.

2. Retrieval Method

2.1. OMEGA Data Set

[8] OMEGA is one of the seven instruments on board the Mars Express spacecraft orbiting around Mars since December 2003. It is an imaging spectrometer analyzing the reflected solar light and the planetary thermal emission [*Bibring et al.*, 2004]. In each resolved pixel (1.2 mrad in the instantaneous field of view) OMEGA acquires a spectrum in 352 contiguous spectral channels from 0.35 to 5.1 μm, with a spectral sampling ranging from 7 nm (in the visible) to 13 nm (from 1.0 to 2.7 μm) and 20 nm (from 2.7 to 5.1 μm).

[9] In the SWIR channel used in this paper, OMEGA operates in the whisk broom mode. Each image pixel is focused by an IR telescope on a slit, followed by a collimator. A scanning mirror in front of the telescope provides cross-track swaths and the spacecraft motion provides the second spatial dimension. Therefore each spectra is obtained using the "same" spectrometer.

[10] Each OMEGA spectral image or "cube" is a stripe of several hundreds of pixel length. Its width depends on the altitude of the spacecraft during the observations: 16, 32, 64, or 128 pixels. For instance, 16 pixels are used for the low-altitude (<350 km), high-resolution ($\simeq$400 m/pixels) observations, whereas the 128 pixels mode is adopted from altitudes above 1500 km to provide wide images with resolution above 2 km/pixel.

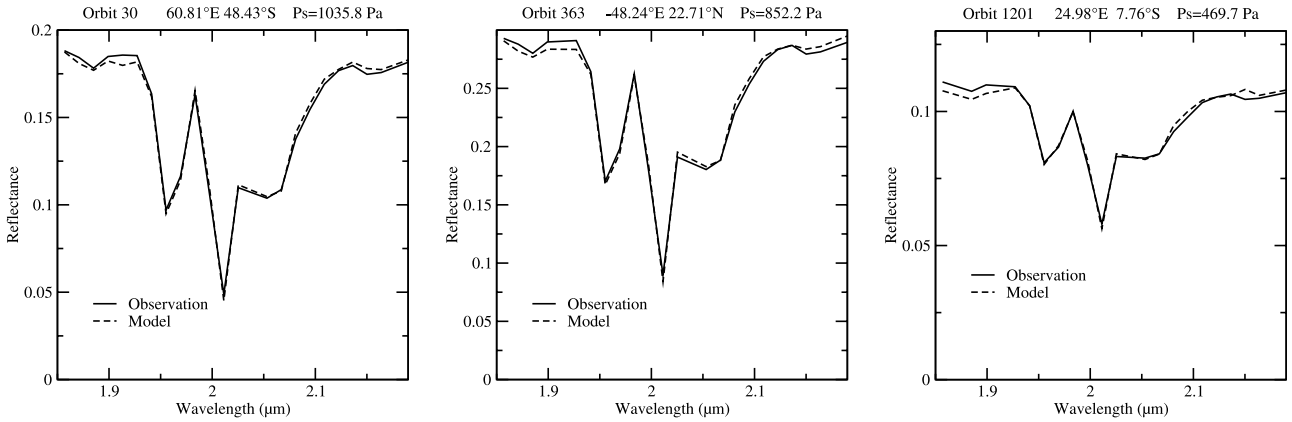

Figure 2. Three typical spectral fits of the OMEGA spectra with various surface pressures. (left) In Hellas Planitia (48.432°S, 60.809°E), orbit 30 (L_s = 335.7°) with a measured surface pressure of 1036 Pa. (middle) The VL1 site observation with the observation conditions detailed in Figure 1 (22.7057°N, 48.237°W), orbit 363 (L_s = 28.2°) with a measured surface pressure of 852 Pa. (right) In Terra Meridiani (7.764°S, 24.980°E) with a measured surface pressure of 470 Pa.

[11] OMEGA has provided the first comprehensive coverage of the Martian surface in the near infrared and visible wavelengths [*Bibring et al.*, 2005, 2006], and has already made possible a lot of discoveries about Mars surface and its history, its polar caps and its atmosphere.

2.2. Outline of the Retrieval Method

[12] Assuming that the CO_2 mixing ratio is known, the hydrostatic surface pressure on Mars is directly proportional to the column amount of CO_2 in the atmosphere. Similarly, the relative band depth observed in the OMEGA spectra at 2 μm is, to first order, proportional to this column amount (Figure 1). It can therefore be used to estimate surface pressure in any pixel. To perform this measurement with a maximum accuracy, however, it is better to separately use the information contained in each OMEGA channels ("spectels") affected by CO_2, and to carefully take into account all the other factors (temperature, aerosols, surface spectrum, instrument response function) which can affect the observed spectra. We chose to focus on the 25 OMEGA spectels between 1.8 and 2.2 μm, a spectral range that includes the 2 μm CO_2 absorption band (stronger absorption bands are available in the OMEGA range near 2.75 and 4.4 μm, but they are usually saturated under Martian conditions at OMEGA resolution). For these 25 spectels, we have developed a complete and accurate forward model to simulate an OMEGA spectrum for any given observing geometry, surface spectrum, atmospheric temperature, aerosol content, and, of course, surface pressure. The surface pressure retrieval is carried out by determining the value of the surface pressure which provides the best fit to the observed spectrum, with the other parameters being estimated from an external source (temperature, aerosol content) or directly from the OMEGA observations (surface spectrum). In practice we perform a best-fit procedure to retrieve the surface pressure and the mean surface albedo. The convergence toward the best fit solution is found using a downhill simplex algorithm to minimize the sum of the squares of the differences between the observed and modeled spectra. The minimization is well defined since the best fit albedo is mostly constrained by the continuum on each side of the CO_2 band whereas the best fit pressure depends on the depth of this band. Tests show that the retrieved pressure is not sensitive to the initial guess.

[13] Three typical example of the spectral fit to the OMEGA spectra are shown in Figure 2. The difference between measurements and model fit is less than 3% (less than 2% in the gas band) except at 2.011 μm where it reaches 6% in Hellas and Meridiani. The possible source of errors are detailed in section 3.

2.3. Atmospheric Radiative Transfer Models

[14] The radiative transfer code used to simulate the CO_2 absorption band from 1.8 to 2.2 μm is based on a line-by-line model described by *Melchiorri et al.* [2006]. The original model is designed to simulate the absorption by CO, H_2O and CO_2 over the entire spectral range observed by OMEGA. We restricted our version to the 1.8 to 2.2 μm range, and made the assumption that the absorption by CO and H_2O would be negligible in this spectral range. This assumption is valid most of the time on Mars, except during the "wettest" season on Mars (northern summer in the northern hemisphere), during which the water vapor absorption band centered at 1.87 μm can become significant. The atmosphere is discretized in 30 plane-parallel layers in $\sigma = p/p_s$ coordinates from the surface up to about 60 km. In each layer, the CO_2 volume mixing ratio is set to 0.953, and the CO_2 line parameters are obtained from the GEISA 2003 database [*Jacquinet-Husson et al.*, 2005] with a collisional broadening coefficient of 0.1 and an exponent of 0.75. The error induced by the uncertainties on these parameters is discussed in section 3.6. The incident solar spectrum is taken from *Colina et al.* [1996]. The model spectral resolution is 8.10^{-3} cm^{-1}. This resolution was carefully chosen in order to ensure a very good accuracy while minimizing computational cost. It is coarser than the resolution theoretically needed to fully resolve all the individual CO_2 lines given their expected Doppler widths, but tests showed that the difference between spectra calculated with this resolution never differ by more than 0.02% from spectra computed with a 10^{-3} cm^{-1} resolution.

Table 1. Parameter Grid of the Look-Up Tables Used by the Fast Radiative Transfer Model Designed to Process the OMEGA Observations[a]

Parameter	Tabulated Grid Values	Interpolation Function
p_s surface pressure (Pa)	50, 150, 180, 215, 257, 308, 369, 442, 529, 633, 758, 907, 1096, 1300, 1500	linear in $\ln(p_s)$
μ_0 cosine of solar zenith angle	0.2, 0.35, 0.52, 0.73, 1.	linear in $e^{-\mu_0}$
μ_1 cosine of viewing angle	0.6, 0.72, 0.85, 1	linear in $e^{-\mu_1}$
ϕ phase azimuth angle (°)	0, 71, 109, 180	linear in $\cos(\phi)$
T_1 temperature at 0.1 scale height (K)	160, 213, 260	linear in $T_1^{1.5}$
T_2 temperature at 4 scale heights (K)	80, 146, 200	linear in $T_2^{1.5}$
Ground albedo	0.05, 0.1, 0.2, 0.3, 0.4, 0.5, 0.6	linear
Dust optical depth	0.05, 0.1, 0.2, 0.3, 0.5, 0.7	linear

[a]A total of 1,814,400 spectra can be interpolated using the interpolation function given in the right column. These functions were chosen to minimize the error resulting from the interpolation. The azimuth angle ϕ is the sun-target-spacecraft angle projected onto the surface, from which the phase angle is derived.

[15] The original *Melchiorri et al.* [2006] model did not include the scattering and absorption by atmospheric dust, which is always significant. Therefore we added a parameterization of the radiative transfer through dust aerosols suitable for line-by-line radiative transfer calculations. This new parameterization is an improved version of the model proposed by *Sobolev* [1975]. A detailed description is given by Forget et al. (A very simple algorithm to compute light scattering in optically thin planetary atmosphere: Application to remote sensing on Mars, submitted to *Geophysical Research Letters*, 2007), who show that, under Martian conditions, the parameterization provides results very close to the well known Spherical Harmonic Discrete Ordinate Method (SHDOM) model [*Evans*, 1998], but with much higher computational speed. We use the single-scattering properties of dust provided by *Ockert-Bell et al.* [1997] and assume that the dust is uniformly mixed (the related uncertainties are discussed in section 3.3). In the present studies we neglect the possible impact of water ice aerosols and select OMEGA observations accordingly, as described by *Spiga et al.* [2007]. Such aerosols could easily be added in the future.

[16] In spite of all these simplifications, such a line-by-line model remains too slow to be used to produce maps of surface pressure. Each OMEGA image contains about 10^5 pixels, and for each pixel, numerous radiative transfer calculations have to be performed to iteratively minimize the distance between modeled and observed spectra. Therefore we used the line-by-line radiative transfer code to build a set of multidimensional look-up tables of spectra from which a spectrum could be quickly derived by multidimensional interpolation. The spectral signature of the atmosphere near 2 μm depends on the following parameters: (1) the surface pressure, (2) geometry angles such as the solar zenith angle, the viewing angle and the phase angle, (3) the atmospheric dust opacity, (4) the surface albedo, and (5) the temperature profile. Each of these parameters had to be represented by one or more dimension in the look-up tables. The parameters grid and the interpolation function were designed to mimic the reference model with a negligible error. These are described in Table 1. Spectra are stored in the tables for 7 surface albedos assuming a "grey" surface. To compute a spectrum with a non-grey surface from the look-up tables (i.e., with a different surface albedo in each spectel to better reproduce Mars surface spectra, as explained in section 3.4), the interpolation in the albedo dimension is performed separately for each spectel.

[17] Representing the temperature profiles with a reasonable number of parameters requires a specific treatment. The 30 parameters corresponding to the temperatures in each layer of our model make it impossible to integrate the full range of temperature profiles in the look-up table. In order to diminish the amount of information needed, we chose to approximate any given input temperature profile by a "radiatively equivalent" simpler profile designed to produce the same spectrum than the original profile, but defined by only two temperatures T_1 and T_2. The first temperature T_1 is the temperature of the input profile at 0.1 scale height above the surface. The simplified profile varies linearly from the surface, through T_1 at 0.1 scale height up to T_2 located at 4 scale heights, above which the temperature is set constant (simulations show that the temperature above 4 scale heights has a negligible impact on the atmospheric spectrum). The value of T_2 is computed by solving the following condition: the vertical integral of the temperature weighted by the pressure $\int_{ps}^{0} T(p)\, p\, dp$ in the simplified profile must be the same than in the input profile. Tests performed with this simplified profile show that the error introduced is less than 0.5% on the CO_2 band depth at 2 μm. Altogether, the total error due to the use of look-up tables rather than the full radiative transfer model is always less than 1.5%, for a computation time 400 times faster. Further tests show that the resulting error on the pressure retrieval is less than 1 Pa.

3. Determination of the Forward Model Input Parameters and Estimation of the Retrieval Errors

[18] The spectral simulation depends on several input parameters which are determined from the OMEGA data set or from other sources. Uncertainties in these parameters result in errors in the retrieved pressure and these have to be explicitly included in the error budget of the retrieval. Below we describe the determination (and the corresponding uncertainties) of these parameters: observing geometry, dust aerosols, atmospheric temperature, surface spectrum and albedo, instrument response function, CO_2 mixing ratio, CO_2 gas spectroscopic parameters. We also

estimate the errors resulting from the instrument noise and biases, and discuss the consequence of neglecting polarization. Finally we estimate the total relative and absolute errors.

3.1. Geometry

[19] The solar zenith angle, the viewing angle and the phase azimuth angle are provided by the Mars Express and OMEGA instrument teams with a precision around 10^{-3} rad. The corresponding error is thus negligible. It could have been non-negligible with very large solar zenith angle or viewing angles. However, in practice, we process OMEGA observations obtained in nadir mode, with viewing angle close to zero, and we select observations with cosine of solar zenith angle lower than 0.6, in order to optimize the signal to noise ratio (see section 3.5 and *Spiga et al.* [2007, section 2.1]). Doing so, we also ensure that no errors are introduced by neglecting the sphericity of the planet in our plane parallel atmosphere model.

3.2. Temperature Profile

3.2.1. Determination of the Atmospheric Temperature

[20] The temperature of the atmosphere cannot be derived from the OMEGA observations. Instead, we use temperature profiles provided by the LMD Mars General Circulation Model (GCM) [*Forget et al.*, 1999] which are available from the Mars Climate Database Version 4.1 [*Forget et al.*, 2006; *Lewis et al.*, 1999]. We used GCM simulations performed assuming the 1999–2001 TES dust opacity ("Martian Year 24"), a year thought to be typical with regards to the dust cycle (see section 3.3). Comparisons with a sample of PFS data obtained simultaneously (OMEGA and PFS often observe the same area) shows that the predicted temperature profiles differ by less than a few kelvin from the PFS temperature retrieval [see, e.g., *Grassi et al.*, 2005, 2007]. More generally, systematic comparison between LMD GCM predicted temperatures and all the temperature profile observed by Mars Global Surveyor radio-occultation experiment show that the model-observation differences follow a bell-shaped normal-like distribution with a standard deviation around 5 K in the low and middle latitudes [*Montabone et al.*, 2006, Figure 7].

[21] GCM temperature fields are computed on a large-scale grid with a resolution of about 200–300 km. Smaller-scale variations of temperature should occur on Mars, in relation with topography slopes or small-scale albedo and thermal inertia variations. They cannot be predicted by the GCM, and may thus affect the pressure retrieval locally. To assess the magnitude of these temperature variations, we analyze the surface temperature field which can be directly derived from the thermal part of the OMEGA spectra [*Jouglet et al.*, 2007]. In most observations, especially in flat areas, we found that the OMEGA surface temperature measurements are very close to the GCM predictions and that local temperature excursions are usually lower than 10 K. Because the exchange of heat between surface and atmosphere are quite limited on Mars, it is likely that the atmospheric circulation will damp the small-scale variations of atmospheric temperature and that they will be smaller than the surface temperature variations. Nevertheless, local temperature variations could create local artifacts in the retrieved pressure fields which have to be taken into account, as discussed by *Spiga et al.* [2007].

3.2.2. Error Due to Temperature Uncertainties

[22] To estimate the error on the surface pressure measurement due to the atmospheric temperature uncertainties, we performed pressure retrievals on a reference spectrum generated with the full line-by-line radiative transfer model, with several temperature profiles. Figure 3 shows the results of such a sensitivity analysis for a reference case which corresponds to an observation of the Viking Lander 1 site by OMEGA (see section 4.1), with observation parameters typical of OMEGA data.

[23] When the inversion algorithm is applied to the reference spectrum generated with the full temperature profile, but with no added error, the retrieved pressure is found to be very close to the input P_s value, with a slight shift of less than 0.3 Pa. This consistency indicates that the use of look-up tables and simplified "radiatively equivalent" temperature profiles give satisfying results, while greatly improving the CPU consumption of the retrieval process. When the inversion algorithm is applied using temperature profiles shifted at every altitudes by errors within ±15 K, we show that an underestimation of 15 K leads to an overestimation of the measured surface pressure of 15 Pa, and vice-versa. This is explained by the fact that increasing temperature enhances the absorption by CO_2 and thus increases the retrieved pressure. Figure 4 illustrates the impact of temperature on an OMEGA-like spectrum. It shows that all the spectels are not affected in the same way and that the side of the strong absorption bands (seen at OMEGA resolution) are more sensitive to temperature than the center of the bands. A more detailed analysis suggests that this is due to the fact that the weaker lines are strengthened with the increasing temperature and widened by Doppler Broadening (Doppler Broadening enhances absorption when the line saturates). In the center of the bands, this effect is counterbalanced by the presence of large saturated lines which tend to get narrower with increasing temperature (the width of such large saturated lines is controlled by Lorentz Broadening which decreases with temperature). Nevertheless, the CO_2 band observed at OMEGA resolution absorbs more photons when the atmosphere is warmer. Heating the atmosphere thus deepens the CO_2 absorption band with respect to the continuum. If the modeled atmosphere is colder than in reality, our algorithm needs to increase the pressure to match the observed spectrum, consistently with Figure 3.

3.3. Dust Radiative Effects

3.3.1. Determination of the Dust Opacity

[24] The optical depth of the atmosphere cannot easily be derived from the OMEGA observations. Unfortunately, it is known to vary in space and time. To estimate the optical depth of the observed scene, we have assumed that the amount of dust in the atmosphere would be close to the value retrieved at the same season (same solar longitude) and the same location in a previous year by the Thermal Emission Spectrometer dust observations at 9.3 μm [*M. D. Smith et al.*, 2001; *Smith*, 2004]. Consistently with the estimation of temperature, we chose to use the opacity obtained between March 1999 and June 2001, a year thought to be typical with regards to the dust cycle. TES

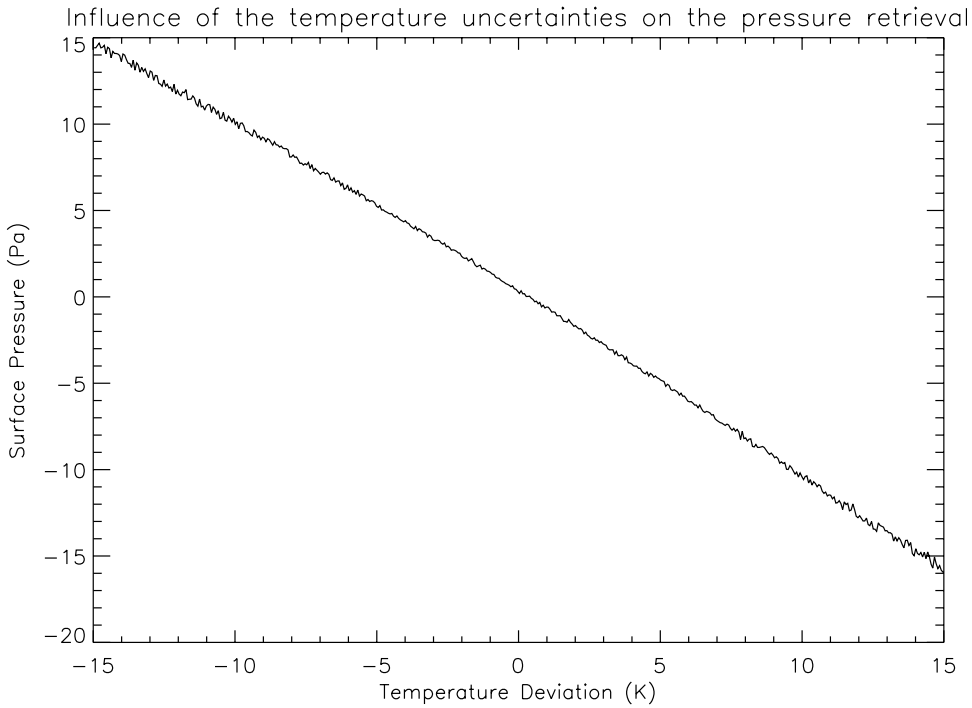

Figure 3. The effect of atmospheric temperature on the surface pressure retrieval. Note that the numerical dispersion due to the minimization is very low. The simulations were performed with the same parameters as in Figure 1, with a reference surface pressure P_s = 822.5 Pa.

observations (only available until 31 August 2004) and THEMIS observations later showed that this year was quite similar to the 2004 year observed by OMEGA, at least after the regional dust storm that affected Mars in January 2004 [*Smith*, 2006]. The TES optical depth at 9.3 μm normalized to the 610 Pa level are scaled to the local surface pressure and multiplied by 1.65 to provide the optical depth at 2 μm. OMEGA observations corresponding to dust optical depth higher than 0.4 are not used. In addition, the actual presence of atmospheric dust is checked qualitatively with color images built with the OMEGA visible channel [see *Spiga et al.*, 2007]. Absolute precision should be better than ±0.2. Within one OMEGA image, the relative variation of dust opacity (scaled to surface pressure) should be significantly lower: far from lifting events (storms) which remain localized in space and time and which can be identified in the OMEGA visible observation if present, dust opacity is observed to slowly vary in time [*Colburn et al.*, 1989; *Wolff et al.*, 2006] and over large distance [*M. D. Smith et al.*, 2001]. In the future, we plan to use the dust opacity retrieval derived from the Mars Express Planetary Fourier Spectrometer (PFS) [e.g., *Zasova et al.*, 2005].

3.3.2. Error Due to Uncertainties on the Dust Radiative Effects

[25] In addition to the error made on the column dust opacity, uncertainties also exist for the dust radiative properties, which control the scaling factor between TES observations at 9.3 μm and OMEGA 2 μm as well as the single-scattering albedo and asymmetry parameter. The opacity derived from TES may also not be exactly proportional to the actual near-infrared opacity if the dust is not uniformly mixed vertically in the first scale height. Furthermore, *Houweling et al.* [2005] showed that variations in the vertical distribution of dust can have a significant impact on the retrieved column CO_2 over the Sahara desert. There, dust is often confined between the first 1–2 km and 3–5 km, with optical depth ranging between 0.1 and ≃1.5. On Mars however, except maybe near lifting regions which remain

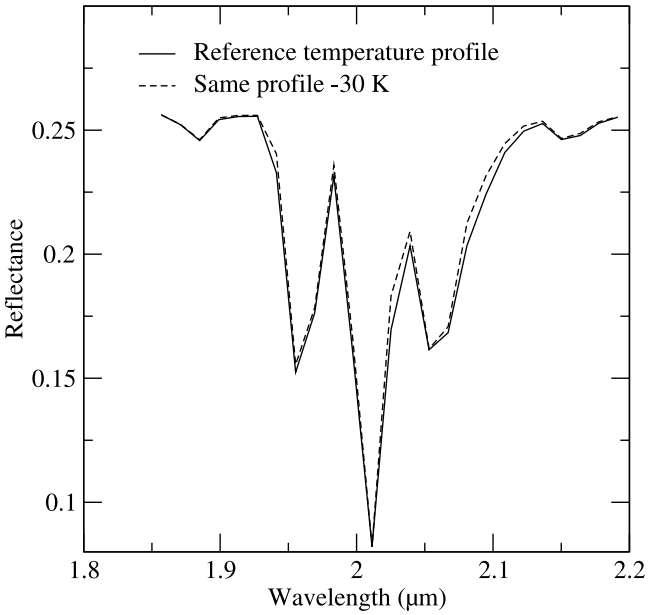

Figure 4. The effect of atmospheric temperature on an OMEGA-like synthetic spectrum. The simulations were performed with the same parameters as in Figure 1, with a reference surface pressure P_s = 822.5 Pa.

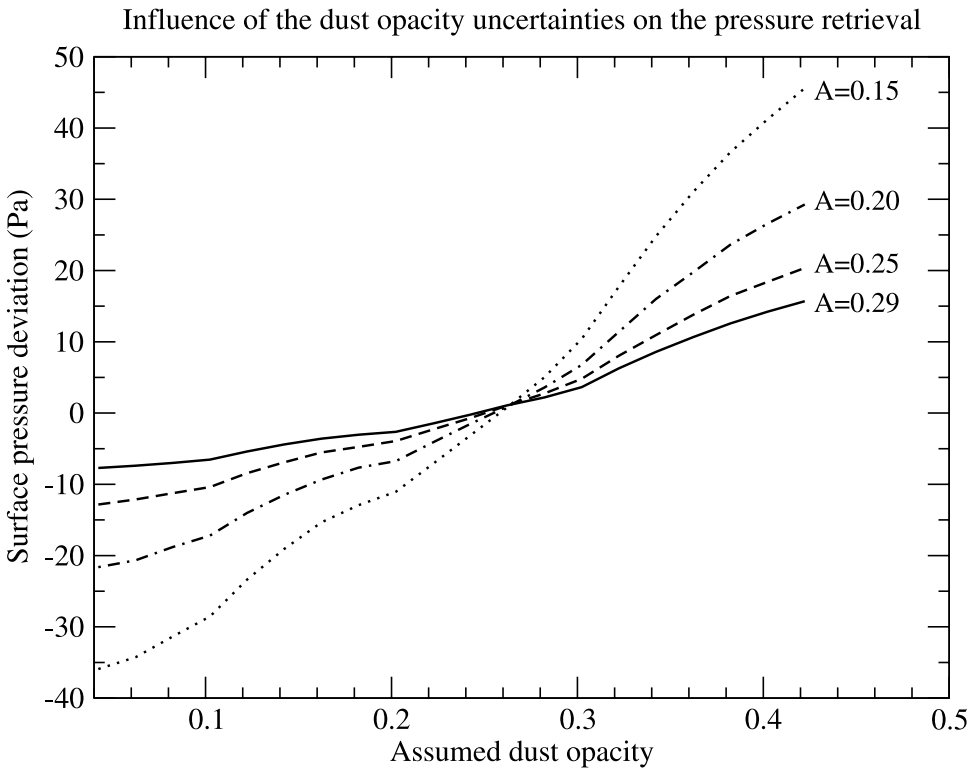

Figure 5. Impact of the uncertainty of the assumed atmospheric dust opacity on the surface pressure retrieval, for various surface albedos A. The simulations were performed with the same parameters as in Figure 1, with a reference surface pressure P_s = 822.5 Pa and a reference opacity of 0.24. The global shape of the curves results from the linear interpolation performed in the look-up table model.

localized in space and time, airborne dust is composed of long-lived small particles which are usually observed [e.g., *Wolff et al.*, 2006; *Montmessin et al.*, 2006] and predicted [e.g., *Newman et al.*, 2002] to be well mixed, at least in the first scale heights which are of relevance here. This effect could be significant in dust lifting regions but, as mentioned above, we can identify and disregard such regions using the OMEGA visible channel. Nevertheless, we have performed retrieval simulations assuming that the dust scale height could be twice or half the atmospheric scale height, and found that the effect on retrieved surface pressure was less than about 1 Pa. Below we assume that the errors resulting from the dust single-scattering optical properties and vertical distribution can be accounted for by an additional uncertainty on the dust opacity.

[26] Figure 5 presents the results of a sensitivity analysis similar to the one carried out with the temperature, performed with τ ranging from 0.04 to 0.44 to process the reference spectrum obtained with τ = 0.24. It shows the calculated pressure retrieval error as a function of the assumed dust optical depth and surface albedo. Underestimating the dust opacity by 0.2 leads to underestimate the pressure by about 7 to 35 Pa, depending on the assumed surface albedo. Increasing the dust opacity tends to lower the CO_2 relative band depth, because the dust scattering of light is relatively more apparent in the absorption band than in the surface continuum. Therefore the measured pressure is underestimated. Toward darker regions, the influence of the dust is stronger. As the surface albedo decreases and the dust optical depth increases, the ratio of the number photons that are reflected from the surface and the atmosphere decreases. Photons that do not traverse the entire path from the top of the atmosphere to the surface provide little or no insight into the surface pressure. The error become especially significant for albedos below 0.17. Fortunately, the fraction of the surface of Mars with such low albedos should be relatively small [see, e.g., *Pleskot and Miner*, 1981], and most of our retrieval are usually performed in brighter regions, where this error remains acceptable, and where the signal to noise ratio is more favorable for our calculations.

[27] Interestingly, the error resulting from the uncertainties on dust opacity should often be anti-correlated with the error introduced by the estimation of atmospheric temperature. This is due to the fact that the same dust observations are used to estimate dust opacity and calculate temperature. For the pressure retrieval, an advantage of this strategy is that any overestimation of the dust opacity will usually lead to an overestimation of the atmospheric temperature. Since dust opacity and atmospheric temperature have opposite effects on the pressure retrieval, the combined error will be reduced.

3.3.3. Impact of Aerosol Polarization

[28] The forward model used to simulate the OMEGA observation neglects polarization effects. However, neglecting polarization has been shown to be a source of error in the case of pressure retrieval on Earth using the 760 nm O_2 absorption band with high-resolution polarization-sensitive instruments like GOME or SCIAMACHY [*Stam et al.*, 1999, 2000]. The sensitivity of GOME and SCIAMACHY to

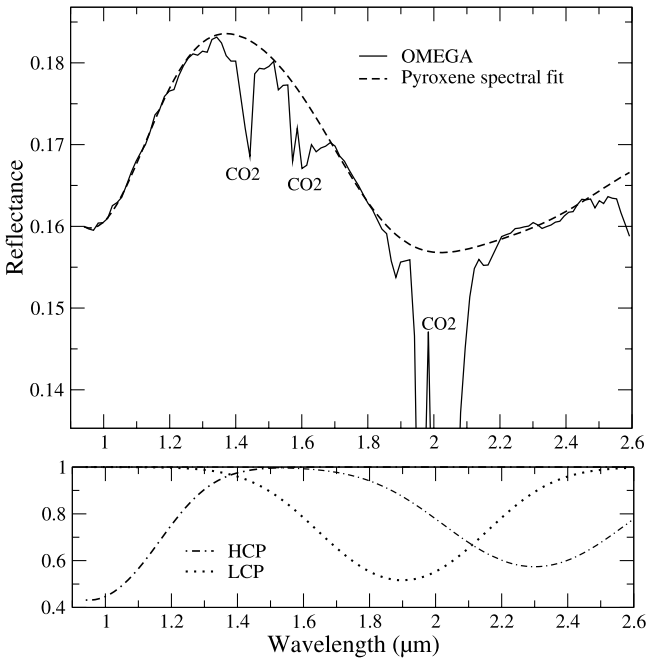

Figure 6. An example of Modified Gaussian Model (MGM) fit of a pyroxene-rich OMEGA surface spectrum assuming that the surface (spectels outside the CO_2 gas bands) is composed of a mixture of high-calcium pyroxenes (HCP) and low-calcium pyroxenes (LCP). The spectrum was obtained on orbit 232 (L_s = 8.7°) in the Syrtis Major area. The "Pyroxene spectral fit" reflectance (top) is obtained in the natural log reflectance space by adding a baseline continuum to three modified Gaussian distributions centered at 1.0, 1.9 and 2.3 μm (bottom) that mathematically describe the known mineral absorption, and the depths of which are adjusted to fit the observed spectrum. This fit is used to predict the shape of the surface spectrum in the 2 μm region.

polarization is mainly due to the use of gratings for spectral dispersion. OMEGA also use gratings but its polarization has not been measured. The possible errors can have several origin. In the presence of polarizing aerosols, the degree of linear polarization of light transmitted through the atmosphere inside an absorption band can deviate significantly from that in the nearby continuum, creating errors in the measured band depth when using a spectrometer sensitive to polarization. Conversely, if the surface is more polarizing than the atmosphere, polarization could affect the continuum more than the line core regions. In the case of CO_2 retrieval with SCIAMACHY using the 1.58 μm absorption band over land with an aerosol loading around 0.2, *Bösch et al.* [2006] estimated that neglecting polarization leads to a maximum error of 0.5%. It is likely that our retrieval with OMEGA is even less sensitive to this effect. Indeed its spectral resolution is much coarser (13 nm versus 0.4 nm for GOME in the O_2 A band and 1.4 nm for SCIAMACHY in the 1.58 μm CO_2 band). As shown by *Stam et al.* [2000] on the basis of atmospheric radiative transfer calculations, the impact of polarization strongly decreases with decreasing spectral resolution. Moreover, telescopic polarimetric observations of Mars [e.g., *Shkuratov et al.*, 2005] suggest that the cloud-free Martian atmosphere is only weakly polarizing. Polarization by water ice clouds can be significant, but we discard observations containing water ice clouds. Thus we believe that neglecting polarization should have a small impact on our results compared to the other uncertainties, although we have to acknowledge that it is difficult to quantify this impact.

3.4. Surface Spectrum and Albedo

3.4.1. Determination of the Surface Spectral Shape

[29] The Martian surface is composed of minerals which can present significant spectral signatures in the near infrared. These signatures can affect the spectra observed by OMEGA, and thus falsify the pressure measurements. The 1.8–2.2 μm wavelength range used here is especially affected by two family of minerals: hydrated minerals and pyroxenes. Hydrated minerals are only observed in few specific locations [*Bibring et al.*, 2005], which are easy to avoid. Pyroxenes, on the other hand, have been mapped by OMEGA and shown to cover significant part of Mars [*Mustard et al.*, 2005; *Bibring et al.*, 2006] in low-albedo regions and old terrains.

[30] OMEGA can discriminate between the high-calcium pyroxenes (HCP) and the low-calcium pyroxenes (LCP) [*Mustard et al.*, 2005; *Bibring et al.*, 2005]. On the basis of laboratory measurements validated by the OMEGA observations, and using the Modified Gaussian Model (MGM) approach [*Sunshine et al.*, 1990], we assume that the spectra of the two kind of pyroxenes can be modeled by a linear continuum combined with two Gaussians centered at 1.9 and 2.3 μm, with a full width at half maximum of 0.5 and 0.56 μm, representing the LCP and HCP bands respectively [*Kanner et al.*, 2007]. To estimate the spectrum of the surface below the atmosphere around 1.8–2.2 μm (which cannot be known directly because of the CO_2 absorption), we fit the OMEGA spectrum outside the gaseous bands between 1.2 and 2.7 μm with this model, and obtain the modeled spectra around 2 μm (Figure 6).

3.4.2. Determination of the Mean Surface Albedo

[31] In practice, we did not use the estimated surface spectrum directly, because it was not fully consistent with our pressure retrieval model (in particular, it does not take dust into account). Instead, we assume that the MGM model only provides the spectral shape, but that the mean surface albedo is a free parameter to be retrieved through a 2 dimension spectral best fit procedure along with the surface pressure as mentioned above. Doing so, we minimize the error resulting from a bad estimation of the dust opacity, and automatically correct for variations in the reflected light due to local slopes or non-Lambertian reflection effect (we assume that the surface is Lambertian). Therefore no errors can theoretically result from uncertainties on the absolute albedo. Further test also shows that our retrieved surface pressure is completely insensitive to the initial guess of the mean albedo value.

3.4.3. Error Due to the Uncertainties of the Surface Spectral Shape

[32] Error can nevertheless result from uncertainties on the shape of the ground spectra. The influence of spectral signature of all possible minerals on the surface is difficult to compute. Nevertheless we can estimate the error associated with the uncertainties on the key minerals low-calcium

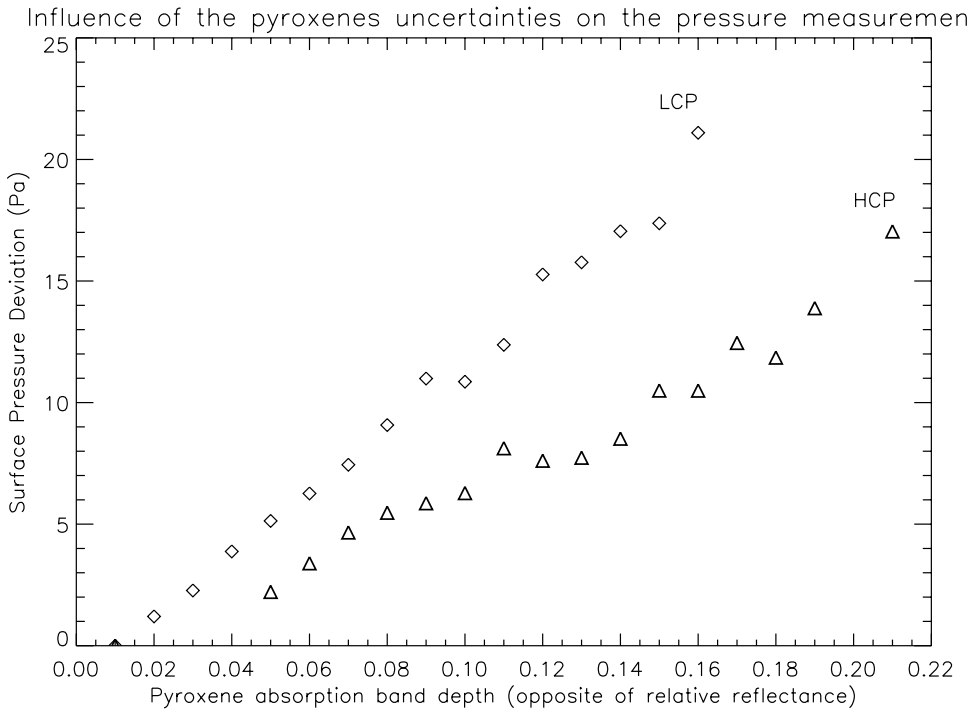

Figure 7. Influence of the presence of surface pyroxene on the surface pressure. The effects of low-calcium pyroxenes (LCP) and high-calcium pyroxenes (HCP) on the observed spectra are simulated with the same parameters as in Figure 1, with a reference surface pressure P_s = 822.5 Pa.

pyroxenes (LCP) and high-calcium pyroxenes (HCP) that we take into account using a Gaussian fit of their spectral signature, as described above. The LCP and HCP absorption band depths (relative reflectances) are empirically known to vary within the respective [0–0.16] and [0–0.21] ranges. The sensitivity of the retrieved pressure (the fit is performed on a reference spectrum as was done before) to the corresponding variations is shown in Figure 7. Underestimating the LCP/HCP radiative influence leads to an underestimation of the pressure. Figure 7 shows that completely neglecting the effect of LCP or HCP in a location where their signature is maximum (which is very rare) would lead to errors reaching 20 Pa. However, the accuracy of the MGM spectral fit is usually better than a few percent [*Mustard et al.*, 2005; *Kanner et al.*, 2007], and we do not expect the pressure error due to the LCP/HCP uncertainties to be higher than a few pascals. Furthermore, as we usually analyze limited areas of OMEGA sessions, the LCP/HCP error, if any, can be regarded as rather homogeneous in the considered area.

3.5. Error Due to Instrument Calibration and Noise

3.5.1. Instrument Noise

[33] OMEGA raw spectral data are radiances in digital number (DN). Values of radiances in the physical units are then obtained using tools provided by the OMEGA instrument team (version SOFT03), which includes a non linearity correction for the detectors and two instrument transfer functions depending on the integration time.

[34] An instrument like OMEGA is read noise limited (photon noise is negligible in comparison). That means that the noise level does not depend on the incoming flux. Purely statistical noise on each spectel signal is 1.85 DN. Values of radiances in the 2 μm band usually range between 200 and 1200 DN, thus OMEGA signal-to-noise ratio (SNR) is in most cases excellent. However, the SNR may not be satisfying for very dark terrains in the infrared. Furthermore, the SNR is known to non-linearly degrade for very bright regions (values of flux between 1200 and 1800 DN). In that range of values, noise may be higher than 1.85 DN, and the amplitude of that noise may vary a lot between brighter (high radiances) and darker (low radiances) zones in a same OMEGA session. Therefore we do not perform pressure retrieval on observations with flux above 1200 DN. When the radiance level is good, statistical comparison of spectra obtained by OMEGA on Mars confirms that read noise dominates the pixel-to-pixel relative error when one considers ratio of flux at various wavelengths, as we do to measure pressure. For instance, spectra obtained in the very flat northern Acidalia Planitia area were found to yield an average 2.011 microns/1.927 microns ratio of 0.27, with a relative variance of 2.08%. This variance can be compared with the theoretical variance of 1,91% that we would have obtained with the 1.85 DN statistical noise. The difference is probably due to altitude variations between pixels since the area is not perfectly flat.

[35] Four ‘‘spectels’’ out of the 25 used in our retrieval are known to be less reliable (mainly because of cosmic ray degradation) and are not taken into account. They are centered at 1.913, 2.039, 2.136 and 2.178 μm.

[36] We can test the pressure measurement sensitivity to the typical OMEGA statistical noise. We start with the above-mentioned simulated reference spectrum and convert it in DN units by inverting the OMEGA transfer function. A ensemble of noisy spectra is then computed. Each noisy spectrum is the initial spectrum with added noise on each

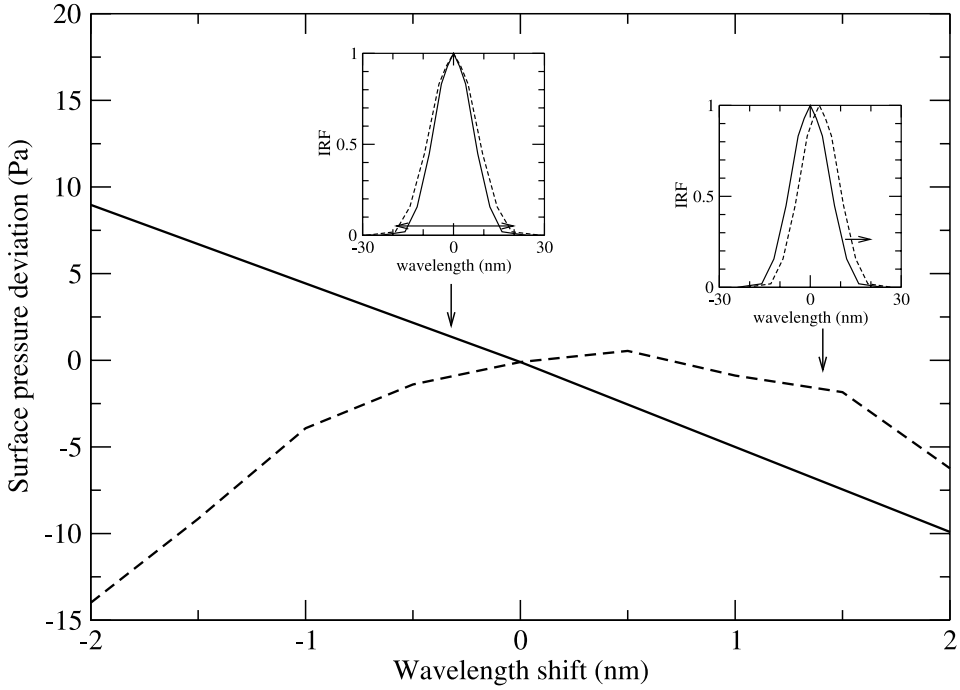

Figure 8. Surface pressure deviation resulting from uncertainties in the instrument response function (IRF) in each OMEGA spectel. Dashed line shows the variation of pressure resulting from a shift in the absolute wavelength reference (the absolute wavelength accuracy is estimated to be better than 1.5 nm). Solid line shows the sensitivity to the width of the IRF, to illustrate the impact of uncertainties on the IRF shape. The simulations were performed with the same parameters as in Figure 1, with a reference surface pressure P_s = 822.5 Pa. The insets show a typical IRF for the OMEGA 0.93–2.73 μm channel used in this paper along with an illustration of the shift used to produce each pressure deviation curve.

spectel reflectances. Noise is randomly defined by the normal Gaussian law with σ = 1.85 DN. The following steps are similar to the usual OMEGA data processing and conversion from DN to physical units. We then test the inversion method on each noised spectrum of the sample. In the end, we get a sample of retrieved ground pressures (normally distributed as expected), and we are able to estimate the standard deviation on surface pressure due to the instrumental statistical noise: ±1.3 Pa, which is very low.

[37] Given that absolute OMEGA calibration is at the 15% level and relative OMEGA calibration is at the 5% level, we also checked the sensitivity of the measurement to an offset applied to the whole spectrum. We found that the offset does not have a significant influence on our measurement (a maximum of 2 Pa for the 15% level), because the pressure retrieval is much more sensitive to relative band depth than to absolute radiance measurement.

3.5.2. Instrument Spectral Calibration

[38] To synthesize an OMEGA spectra with our model, the instrument spectral resolution and spectral sampling is simulated by convolving the calculated, highly resolved modeled spectra with the instrument response function (IRF) in each spectel. For this purpose, the IRF has to be known as accurately as possible. With OMEGA, we have benefited from an excellent ground calibration campaign which was made possible by the long delay between the completion of the flight model of OMEGA in 1995 and its actual delivery to the Mars Express integration team in 2002 (the Mars Express OMEGA instrument is one of two models built for the Russian mission Mars 96, following Russian Space Agency policy at the time). This time was used to perform an in-depth calibration with a particular effort for spectral calibration [*Bonello et al.*, 2005] using a monochromator. After launch and in orbit, possible variations have been investigated using Earth spectra and Martian observations of sharp CO_2 and water ice lines [*Langevin et al.*, 2007]. No changes could be detected throughout the mission in the 0.93–2.73 μm channel used in this paper. The absolute wavelength accuracy is estimated to be better than 1.5 nm. A bias in absolute wavelength would systematically shift the IRF of all spectels and thus affect the surface pressure measurement. The dashed line on Figure 8 shows the error on retrieved surface pressure resulting from such a bias. Interestingly, it appears that the OMEGA spectral grid is such that in most cases, a bias in the wavelength reference leads to an underestimation of the surface pressure (by 2 Pa if the spectel wavelengths are 1.5 nm longer than expected, and by 9 Pa in the opposite case).

[39] The relative wavelength accuracy during the calibration was considerably better thanks to the constant scanning step of the monochromator [*Bonello et al.*, 2005]. The IRFs could thus be determined for each spectel with high precision, with a 4 nm resolution. The shape of the IRFs were found to be similar in each spectel in the 0.93–2.73 μm OMEGA channel, with a slight sensitivity to variations in the spectrometer and detector temperatures. Fortunately, these temperatures are stabilized by thermal control systems

using cryocoolers (for the detector) and a conductive link to a radiator (for the spectrometer). They are constantly monitored when OMEGA is operating. During nominal operations, they are usually very close to their optimal temperature, as expected. Nevertheless, to evaluate the possible bias in retrieved surface pressure resulting from an error in the exact shape of the IRF, we have performed retrieval simulations with several IRF width in each spectel (the width here is defined as twice the full-width at half maximum of the IRF). The solid line on Figure 8 shows that a 2 nm variation in the IRF width (corresponding to the total uncertainty resulting from the thermal variations and the spectral sampling) can lead to a 10 Pa bias in the pressure retrieval. Overall, we can conclude that the error resulting from the uncertainties in the spectral calibration and in the instrument response function should be a systematic bias of less than 20 Pa.

3.6. Error Due to Uncertainties in the CO_2 Mixing Ratio and Spectroscopic Data

[40] In our retrieval, we assume that the CO_2 volume mixing ratio is 0.953. The best measurement of the actual mixing ratio of CO_2 on Mars remains the value retrieved from the Viking mass spectrometer at the beginning of the Viking Lander missions in early northern summer: 0.9532 [*Owen et al.*, 1977]. This mixing ratio is expected to vary with season due to the condensation and sublimation of a significant part of the atmospheric CO2 into the seasonal polar caps. Estimations of the total atmospheric mass variations performed by simulating the Viking Lander surface pressure with a General Circulation Model [*Hourdin et al.*, 1995] suggest that the mean surface pressure can reach extrema corresponding to 0.9 and 1.12 times the mass of the early northern summer atmosphere observed by Viking. These values correspond to a CO_2 mixing ratio ranging between 0.948 and 0.958, depending on the season. For a given partial pressure measured by OMEGA, the associated pressure systematic bias can thus reach ±0.5% (i.e., ±4 Pa for a retrieved P_s = 800 Pa). In fact, this is probably an overestimation of the actual bias. It has been shown that the atmosphere above the condensing polar caps is strongly enriched in Argon [*Sprague et al.*, 2004]. This suggests that a large fraction of the non-condensable gas left behind by the CO_2 condensation remains in the polar regions and does not dilute the CO_2 gas at other latitudes as much as we assumed in the simple calculation above.

[41] The spectroscopic line parameters for the CO_2 2 μm band have been taken from the GEISA 2003 database [*Jacquinet-Husson et al.*, 2005] with a collisional broadening coefficient of 0.1 and an exponent of 0.75 [*Arie et al.*, 1987]. Tests performed with the same line-by-line model, but using HITRAN 2004 [*Rothman et al.*, 2005] for all line parameters including collisional broadening yielded differences at OMEGA resolution of less than 0.04% and 0.01% for CO_2 pressure of 10 and 3 hPa, respectively. However, improved line strengths and positions has just been released by *Toth et al.* [2006], and will be used in the future. For the present studies, *Toth et al.* [2006] suggest that line strength errors below or around 2% on average can be expected for the relatively recent spectroscopic measurement used here. We have performed sensitivity studies to assess the impact of variations in the strength and width of the CO_2 lines. A systematic 2% increase of all the line strengths induces a change in the band depth (at OMEGA resolution) of about 0.5% in the side bands peaking at 1.95 and 2.05 μm and 1.2% in the 2.01 μm central band. Similarly, a 2% increase of all the line widths induces a 0.5% change in OMEGA band depth. On this basis, we estimated that uncertainties on the spectroscopic line parameters correspond to an additional systematic bias of 1% at most (e.g., ±8 Pa for a retrieved P_s = 800 Pa).

3.7. Estimation of the Total Error

[42] From the above calculations, two kind of errors can be identified. On the one hand, a systematic bias, nearly constant throughout the mission or at least during a season, may affect the pressure measurement. It is mostly due to uncertainties (1) in the instrument response functions absolute spectral position ($\leq$1.2%) and exact shape in each spectel ($\leq$1%, see section 3.5), (2) in the spectroscopic line parameters (<1%, see section 3.6), and (3) in the CO_2 mixing ratio (<0.5%, see section 3.6). The total systematic bias should thus be significantly lower than 4% (e.g., ~30 Pa for a retrieved P_s = 800 Pa). On the other hand, from one OMEGA image to another OMEGA image and even within the same OMEGA image, relative errors may result from more variable sources of errors, due mostly to instrument noise, surface spectral shape, atmospheric temperatures and aerosol content. Estimating the combined relative error is especially important to interpret spatial structure in the surface pressure fields, as done by *Spiga et al.* [2007]. To evaluate the total relative error, we performed a Monte Carlo error analysis [*Press et al.*, 1992] by (1) generating an ensemble of spectra for an input pressure P_s affected by the variable uncertainties described above, (2) applying our pressure retrieval algorithm on these spectra, and (3) computing the standard deviation of the retrieved surface pressures compared to P_s. For this purpose, we chose to describe all the input parameter uncertainties with a normal distribution as for the instrumental noise. As mentioned in section 3.2, such a shape is observed when calculating the difference between model prediction and accurate radio-occultation observations [*Montabone et al.*, 2006].

[43] If X is one of these input parameters, the sample computed with the normal Gaussian distribution is $\{X_i\}_{i=0\ldots N}$, where N is the sample extension (we use N = 10,000) and X_i are random values obeying the following normal probability density function:

$$f(x;\mu,\sigma) = \frac{1}{\sigma\sqrt{2\pi}} e^{-\frac{(x-\mu)^2}{2\sigma^2}} \quad (1)$$

where μ is the mean of the sample and σ the standard deviation. In our Monte Carlo analysis, μ is the true value of X and σ is determined from the uncertainty ΔX on the parameter X. As a well-known normal law property states that 99.7% of the excursions of the value from the mean are under three standard deviations, in order to get sample X_i values normally distributed within $X \pm \Delta X$, we set $3\sigma = \Delta X$.

[44] Uncertainties on the following parameters are included: temperature T, optical depth τ, and OMEGA statistical noise (DN). Errors on the pyroxenes diagnostic were not taken in account for technical reasons but are

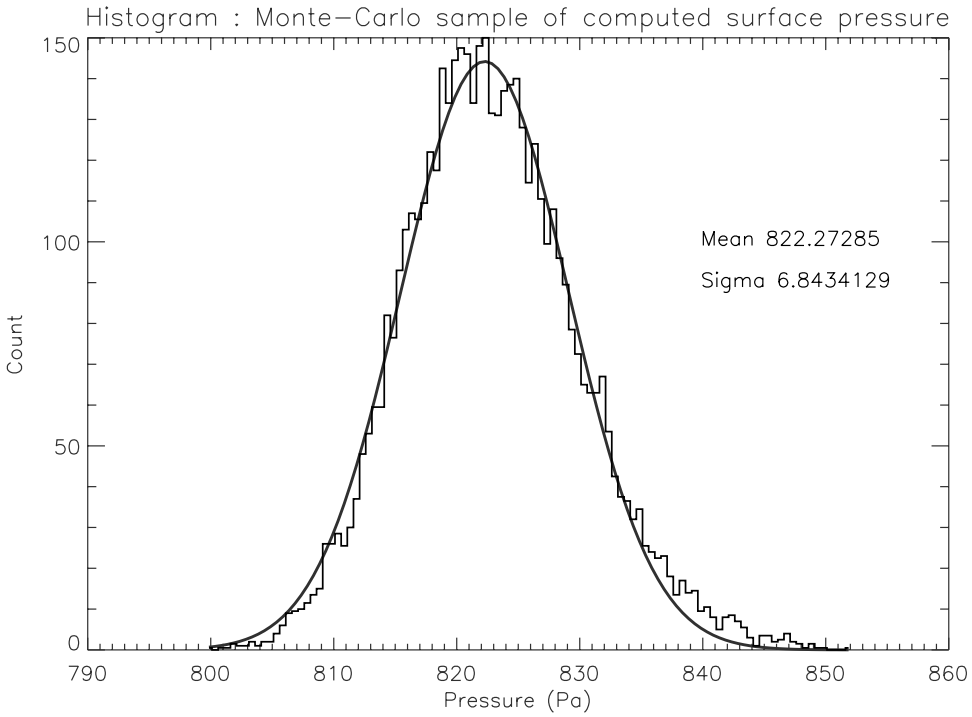

Figure 9. The distribution of 10,000 surface pressure retrievals simulated with the same parameters as in Figure 1 and P_s = 822.511 Pa, except that the synthetic spectra used in the retrieval were randomly affected by errors on the atmospheric temperature and the dust optical depth as well as by instrumental noise (see text). The histogram is shown with a resolution 0.5 Pa.

expected to be small (see section 3.4). Uncertainties amplitudes are similar to the ones prescribed in the previous sections: respectively ΔT = 15 K, $\Delta\tau$ = 0.2, $\Delta DN = 1.85 \times 3 = 5.55$ DN.

[45] In the end, a distribution of retrieved surface pressures is obtained, and its standard deviation can be evaluated. The results obtained for our reference case is shown on Figure 9. The distribution appears normal, suggesting that nonlinearities arising from the inverse method processes are small. The standard deviation of retrieved surface pressure (i.e., the 1-σ relative error) is $\sigma \sim 7$ Pa. corresponding to a 3σ total uncertainty of ±21 Pa. As explained in section 3.3 and 3.5, the error due to dust and noise increase with decreasing surface albedo. A similar error estimation yielded a 1-σ relative error of 10 Pa for a surface albedo of 0.2, and even 15 Pa for a surface albedo of 0.15 (note that we avoid processing area with albedo lower than 0.18).

4. Results and Comparison With Surface Measurements

4.1. Comparison With Viking Lander Records

[46] Ideally, our remote pressure measurements should be validated against ''ground truth'', in situ measurements. No such measurements were performed during the Mars Express mission (there is no pressure sensor aboard the Mars Exploration Rovers). Nevertheless, assuming that pressure is primarily controlled by season and local time, and that the mass of the Mars atmosphere has not varied for thirty years, we can compare with previous lander missions: the Viking Lander 1 and 2, and Pathfinder. Pressure records were obtained by the Viking Lander 1 (22.269°N, 312.050°E) for 2245 sols (more than 3 Martian years) in 1976–1982, and by Viking Lander 2 (47.668°N, 134.282°E) for 1050 sols (almost 2 Martian years) in 1976–1978 [*Hess et al.*, 1980; *Tillman*, 1988]. During summer 1997, Pathfinder (19.010°N, 326.747°E) also transmitted surface pressure measurements [*Schofield et al.*, 1997], but only for 83 sols, covering only a fraction of a Martian year, between L_s = 142° and L_s = 188°. As we write this paper, OMEGA has observed the Pathfinder landing site three times (orbit 511, 2460 and 2493), but none of these observations were performed at the same season than the pressure records. The OMEGA data set also contains some observations of the Viking Lander 2 site (orbit 2374). However, this measurement was obtained during northern winter (L_s = 326°), and the pressure retrieval is not possible because of the low insolation (solar zenith angle >60°) and the presence of polar hood clouds. Finally, the Viking Lander 1 site was observed by OMEGA with good illumination conditions during orbit 363 session 3 (L_s ~28.2° and local time ~10.7 Martian hours). Unfortunately, a part of the OMEGA image is covered by water ice clouds, and we suspect that a thin ice haze might affect the pixel containing VL1 (atmospheric ice tends to make us overestimate surface pressure because of a water ice absorption band centered near 2 μm). Nevertheless, a pressure retrieval at this pixel was possible and gave 852 Pa, to be compared with 831 Pa measured by VL1. Note that the VL1 data were digitized with a 9 Pa quantization interval [*Hess et al.*, 1980]. The measurement uncertainty is thus at least 5 Pa. Nevertheless, remarkably, VL1 recorded the same value for the three consecutive years, (except maybe the third year for which

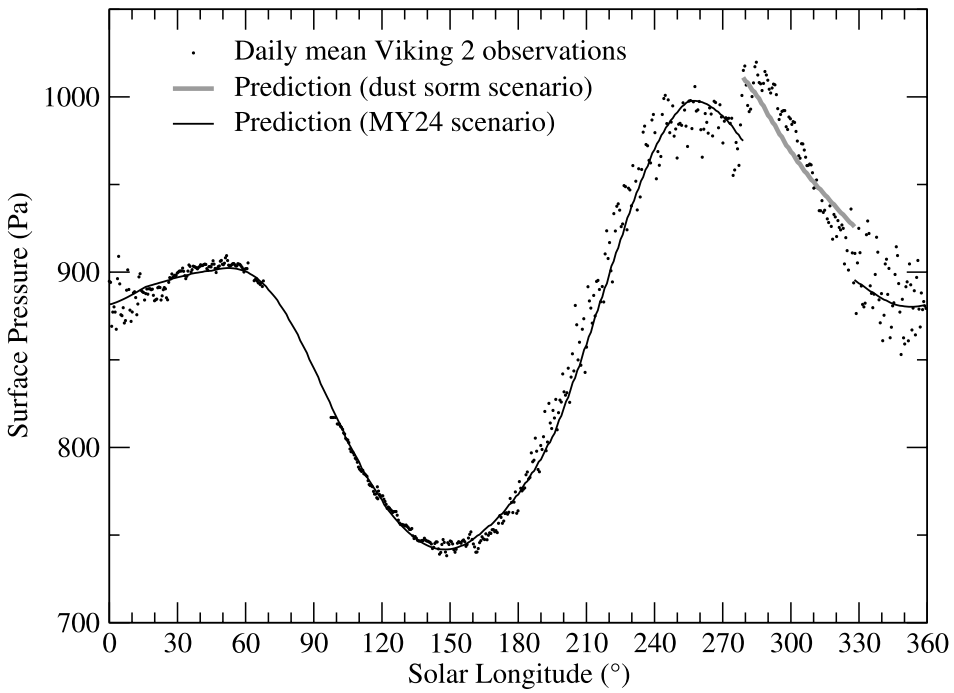

Figure 10. Seasonal variations of the ground pressure at the Viking Lander 2 site. The dots show the daily averaged pressure measurements achieved by the sensor on the lander. The sudden rise of pressure between L_s = 270° and L_s ~330° results from the dynamical effect of the 1977-b global dust storm [*Hourdin et al.*, 1993]. The thin black line shows the output of our surface pressure predictor assuming the standard "Martian Year 24" (MY24) dust scenario. The thick grey line was produced by the predictor assuming a much dustier atmosphere (dust opacity of 4). It shows that the model can accurately predict surface pressure variations resulting from large-scale dynamical processes.

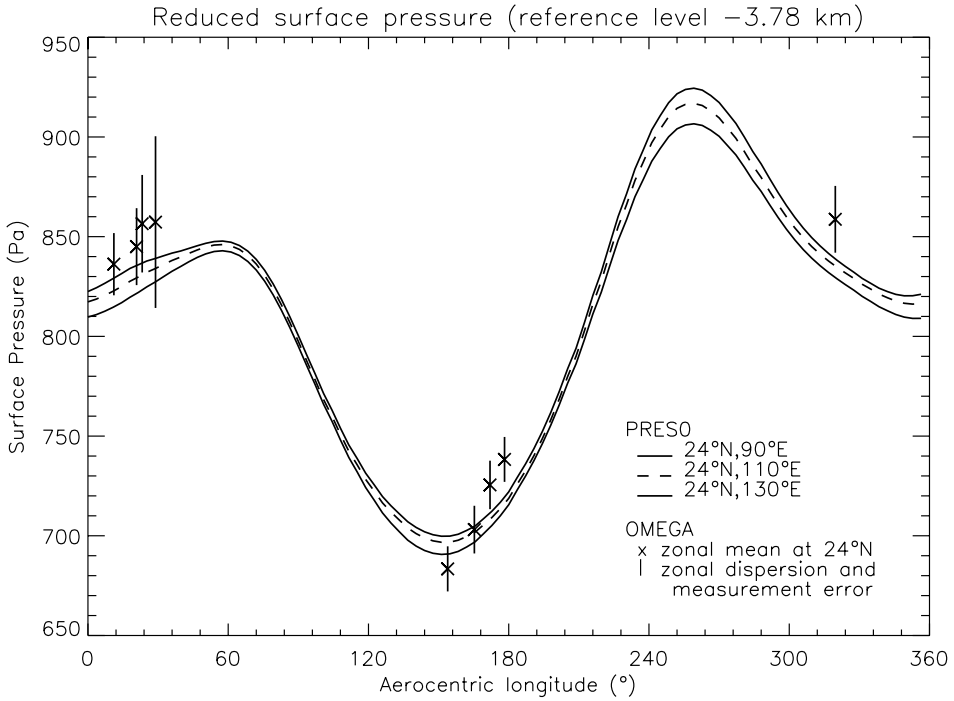

Figure 11. Seasonal variation of the surface pressure in a selected area of Isidis Planitia around 24°N between 90°E and 130°E. Surface pressure measurements retrieved from OMEGA observations (dots) are compared to results from our surface pressure predictor (lines). The error bars illustrate the range of pressure within one OMEGA image at 24°N, extended by 7 Pa on each side to illustrate the 1-σ measurement relative error due to noise, temperature, and dust loading variations. Pressures are scaled to the reference level −3.78 km using the barometric formula as detailed by *Spiga et al.* [2007].

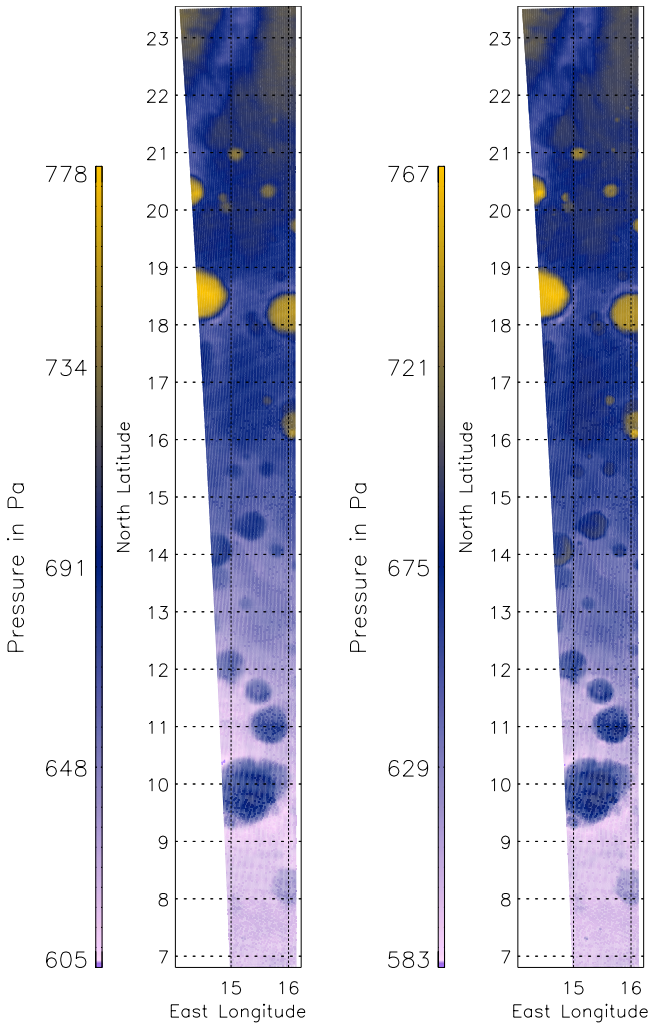

Figure 12. (left) Surface pressure retrieved from the OMEGA observations compared to (right) a synthetic map produced by our surface pressure predictor notably based on the MOLA topography, which is very well reproduced by the OMEGA retrieval.

the local time of the OMEGA observation is included between a 840 Pa and a 831 Pa measurement), suggesting that it is reasonable to compare the year observed with OMEGA with the Viking observations.

[47] In spite of the possible presence of a thin water ice haze, we conclude that the OMEGA measurement is within 2.5% of the ground truth, with a slight overestimation.

4.2. Building a Surface Pressure Predictor

[48] The pressure measurement check at the VL1 pixel, though useful preliminary test, is inadequate for a more general validation of the method. In particular, to validate our retrieved pressure maps, we needed a tool able to predict a reference ground pressure field with full spatial and temporal coverage. Surface pressure at any locations on Mars can be predicted by interpolating the Viking Lander 1 record vertically thanks to the accurate MOLA topography [*D. E. Smith et al.*, 2001]. However, surface pressure is also expected to vary across the planet because of large-scale pressure gradients resulting from the general circulation and the global thermal structure [*Hourdin et al.*, 1993]. To account for this component (including the thermal tides), we used the large-scale surface pressure gradients simulated by the LMD Mars General Circulation Model [*Hourdin et al.*, 1993; *Forget et al.*, 1999] which are available from the Mars Climate Database Version 4.1.

[49] In practice, pressure is derived from the surface pressure fields produced by the GCM, with a vertical interpolation from the coarse GCM topography grid to the high-resolution MOLA grid, and a correction to perfectly match the seasonal variations at VL1 site. The best possible guess of surface pressure P at a given location and time is given by

$$P = P_{\mathrm{GCM}} \frac{\langle P_{\mathrm{VL1_{OBS}}} \rangle}{\langle P_{\mathrm{VL1_{GCM}}} \rangle} e^{-(z-z_{\mathrm{GCM}})/H} \tag{2}$$

with P_{GCM} the pressure predicted by the GCM at the same location and time (interpolated from the GCM grid), $\langle P_{VL1_{\mathrm{OBS}}} \rangle$ the VL1 surface pressure records smoothed to remove thermal tides and transient waves, taken from *Hourdin et al.* [1995], $\langle P_{\mathrm{VL1_{GCM}}} \rangle$ the similarly smoothed VL1 surface pressure predicted by the GCM (properly interpolated vertically and horizontally). z is the altitude of the local surface retrieved from the MOLA data set, and z_{GCM} is the altitude at the location interpolated from the coarse GCM topography grid. H is the scale height used in the hydrostatic equation to vertically interpolate the pressure: $H = RT/g$ with $R = 192$ m^2 s^{-2} K^{-1} the gas constant, $g = 3.72$ m s^{-2} the acceleration of gravity, and T the atmospheric temperature extracted from the GCM at 1 km above the surface. The choice of the 1 km altitude to interpolate surface pressure on Mars is based on the theoretical considerations and tests described by *Spiga et al.* [2007]. This surface pressure predictor is included in the Mars Climate Database V4.1 under the name "pres0".

[50] Figure 10 shows the predicted pressure at the Viking Lander 2 site compared to the actual observations. The agreement is good. The dynamical pressure increase resulting from the 1977-b global dust storm between $L_s = 270°$ and $L_s = 330°$ can be well reproduced by assuming a dusty atmosphere at that time. Our pressure predictor does not include the effect of baroclinic waves (on purpose) which are especially strong in fall and winter at the VL2 latitude and explain the larger amplitude of the waves at these seasons. Nevertheless, the predictor includes the thermal tides, and a detailed analysis shows that the phase and amplitude of the modeled tidal pressure oscillations match the observations.

4.3. Seasonal Evolution

[51] As seen in Figure 10, the evolution of the surface pressure at a given location is characterized by a strong seasonal cycle resulting from the condensation and sublimation of the CO_2 atmosphere in the polar caps. These seasonal variations are not easy to monitor with the OMEGA instrument, because the primary objective of OMEGA has naturally been to observe as many areas as possible. Therefore most locations have not yet been observed more than one to three times.

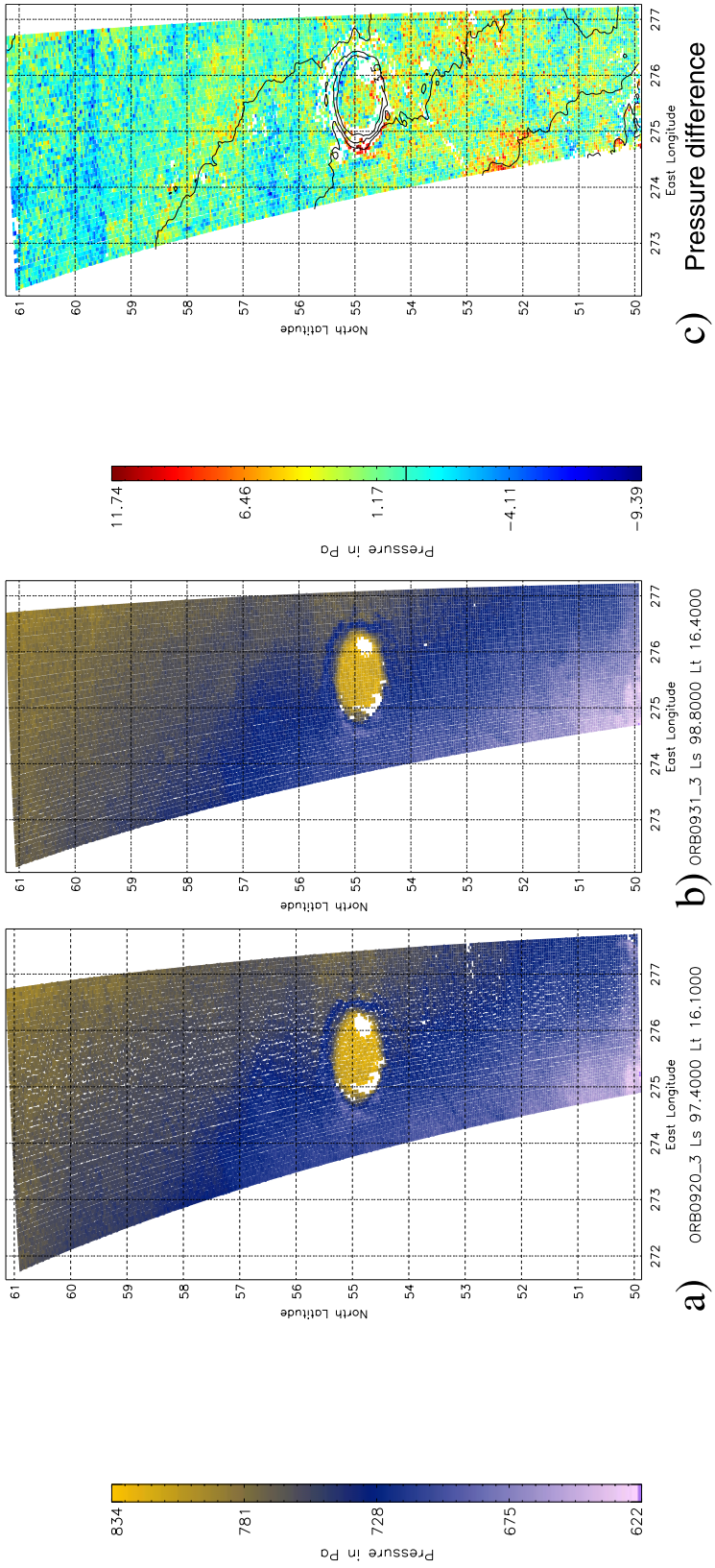

Figure 13. A comparison between two pressure maps retrieved in the same area from two different orbits, three days apart. (a) Pressure map retrieved from orbit 920 at L_s = 97.4° and local time ~16.1 Martian hours. (b) Pressure map retrieved from orbit 931 at L_s = 98.8° and local time ~16.4 Martian hours. (c) A map of the difference, with superimposed topography (black contours).

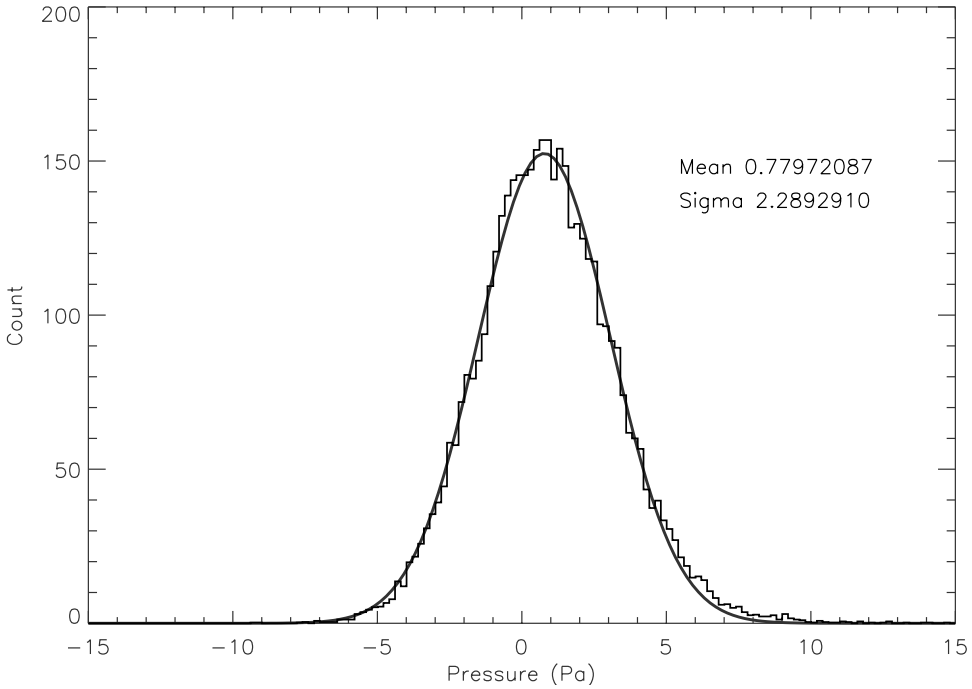

Figure 14. A histogram illustrating the bell-shaped distribution of the differences in pressure retrieval from each pixel shown in Figure 13c.

[52] Nevertheless, by selecting pressure measurements obtained in a flat region at about the same latitude, we were able to monitor the seasonal cycle of surface pressure at 24°N in Isidis Planitia (Figure 11), in good agreement with the surface pressure predictor. There again, such a result gives a confidence in both the relative and absolute surface pressure measurements performed with OMEGA.

4.4. Pressure Mapping

[53] The use of look-up tables and simplified models has allowed us to process numerous OMEGA sessions. In a companion paper, *Spiga et al.* [2007] present several of these maps along with analyses of the meteorological signatures contained in these data. In Figure 12, we show a typical example (among many others) of such a map along with a synthetic map produced by our surface pressure predictor. As expected, the observed pressure field is primarily controlled by the surface topography. The absolute and relative agreement between the observed and expected pressure maps is good, even if a slight overestimation is usually observed in the OMEGA data. This shift is detected in most of the "correct" OMEGA sessions (i.e., the ones that passed a preliminary quality control); its amplitude is different on each example, and may vary from 10 Pa to 30 Pa.

[54] Figures 13a and 13b display two pressure maps retrieved in the same area in the northern plains from two different orbits, three sols apart. The two maps are quantitatively very similar. The mean pressure difference between the two maps is 0.78 Pa with local deviations reaching ±7 Pa. Interestingly, the distribution of the differences follows a bell-shaped distribution (Figure 14) with a standard deviation near 2.3 Pa, as expected for two OMEGA images obtained with similar observing conditions. Figure 13c shows a map of the difference between the two observations. Some structures can be observed, apparently perpendicular to the topography slope. However, their amplitude is so small that it is not possible to attribute their origin to local pressure variations rather than atmospheric dust or temperature fluctuations.

5. Conclusion

[55] Using the OMEGA observations of the CO_2 band centered at 2 μm, we have developed a retrieval algorithm to measure surface pressure from Mars orbit. The algorithm and its input parameters (atmospheric temperature and opacity, surface spectral shape) have been designed to combine high accuracy with efficiency in order to be able to process the hundred of thousands of spectra that are available in each OMEGA image and produce maps of surface pressure. We estimate the 1-σ relative error to be around 7 to 10 Pa depending on the surface albedo, with a possible systematic bias on the absolute pressure lower than 30 Pa (4%).

[56] Such an accuracy allows us to monitor the seasonal variations of pressure in a given location on Mars. The relative accuracy from pixel to pixel should be significantly lower than the number given above, because the bias induced by an error in dust loading or atmospheric temperature should be similar from pixel to pixel. After removal of the topography signal, this allows us to monitor weather patterns, as presented in the companion paper by *Spiga et al.* [2007].

[57] In the future, we plan to improve the accuracy of the measurements by using the temperature profile and aerosol content measured by the Planetary Fourier Spectrometer also on board Mars Express [*Grassi et al.*, 2005; *Zasova et al.*, 2005], and recently released improved spectroscopic

line parameters. In addition, we will benefit from additional observations obtained above the Viking landers and Pathfinder sites, which will provide additional "ground truth" measurements crucial to validate and calibrate the absolute measurements. Finally, more observations of the same area with a few days interval will soon be available. They will allow us to monitor the signature of transient waves in the surface pressure field.

[58] **Acknowledgments.** We thank B. Bezard, T. Fouchet, and E. Lellouch for their assistance with the radiative transfer code development and calibration, E. Millour and L. Montabone for their help, and S. Rodin and two anonymous reviewers for very constructive reviews that significantly improved the content of this article. A part of this work was performed while F. Forget and B. Dolla were visiting the Space Science Division of NASA Ames Research Center (F.F. as a Senior National Research Council fellow). We wish to thank in particular R. M. Haberle along with G. Gibert, J. Hollingsworth, J. Schaeffer, T. Colaprete, and C. P. McKay for their support and advice. We finally thank the OMEGA and Mars Express engineering teams for their excellent work and support.

References

Arie, E., N. Lacome, and A. Levy (1987), Measurement of CO_2 line broadening in the 10.4-micron laser transition at low temperatures, *Appl. Opt.*, *26*, 1636–1640.

Barton, I. J., and J. C. Scott (1986), Remote measurement of surface pressure using absorption in the oxygen A-band, *Appl. Opt.*, *25*, 3502–3507.

Bibring, J.-P., et al. (1991), Topography of the Martian tropical regions with ISM, *Planet. Space Sci.*, *39*, 225–236, doi:10.1016/0032-0633(91)90146-2.

Bibring, J.-P., et al. (2004), OMEGA: Observatoire pour la Minéralogie, l'Eau, les Glaces et l'Activité, in *Mars Express: The Scientific Payload*, edited by A. Wilson, *Eur. Space Agency Spec. Publ.*, *ESA-1240*, 37–49.

Bibring, J.-P., et al. (2005), Mars surface diversity as revealed by the OMEGA/Mars Express observations, *Science*, *307*, 1576–1581, doi:10.1126/science.1108806.

Bibring, J.-P., et al. (2006), Global mineralogical and aqueous Mars history derived from OMEGA/Mars Express data, *Science*, *312*, 400–404, doi:10.1126/science.1122659.

Bonello, G., J.-P. Bibring, A. Soufflot, Y. Langevin, B. Gondet, M. Berthé, and C. Carabetian (2005), The ground calibration setup of OMEGA and VIRTIS experiments: Description and performances, *Planet. Space Sci.*, *53*, 711–728, doi:10.1016/j.pss.2005.02.002.

Bösch, H., et al. (2006), Space-based near-infrared CO_2 measurements: Testing the Orbiting Carbon Observatory retrieval algorithm and validation concept using SCIAMACHY observations over Park Falls, Wisconsin, *J. Geophys. Res.*, *111*, D23302, doi:10.1029/2006JD007080.

Colburn, D. S., J. B. Pollack, and R. M. Haberle (1989), Diurnal variations in optical depth at Mars, *Icarus*, *79*, 159–189.

Colina, L., R. C. Bohlin, and F. Castelli (1996), The 0.12–2.5 micron absolute flux distribution of the Sun for comparison with solar analog stars, *Astron. J.*, *112*, 307, doi:10.1086/118016.

Crisp, D., et al. (2004), The Orbiting Carbon Observatory (OCO) mission, *Adv. Space Res.*, *34*, 700–709, doi:10.1016/j.asr.2003.08.062.

Dubuisson, P., R. Borde, C. Schmechtig, and R. Santer (2001), Surface pressure estimates from satellite data in the oxygen A-band: Applications to the MOS sensor over land, *J. Geophys. Res.*, *106*, 27,277–27,286.

Evans, K. F. (1998), The spherical harmonics discrete ordinate method for three-dimensional atmospheric radiative transfer, *J. Atmos. Sci.*, *55*, 429–446.

Forget, F., F. Hourdin, R. Fournier, C. Hourdin, O. Talagrand, M. Collins, S. R. Lewis, P. L. Read, and J.-P. Huot (1999), Improved general circulation models of the Martian atmosphere from the surface to above 80 km, *J. Geophys. Res.*, *104*, 24,155–24,176.

Forget, F., et al. (2006), The new Mars climate database, paper presented at Second Workshop on Mars Atmosphere Modelling and Observations, Cent. Natl. d'Etudes Spatiales, Granada, Spain.

Fournier, N., P. Stammes, M. de Graaf, R. van der A, A. Piters, M. Grzegorski, and A. Kokhanovsky (2006), Improving cloud information over deserts from SCIAMACHY Oxygen A-band measurements, *Atmos. Chem. Phys.*, *6*, 163–172.

Gendrin, A., S. Erard, P. Drossart, and R. Melchiorri (2003), Observation of pressure variations in the Martian atmosphere, *Geophys. Res. Lett.*, *30*(23), 2227, doi:10.1029/2003GL018234.

Grassi, D., C. Fiorenza, L. V. Zasova, N. I. Ignatiev, A. Maturilli, V. Formisano, and M. Giuranna (2005), The Martian atmosphere above great volcanoes: Early planetary Fourier spectrometer observations, *Planet. Space Sci.*, *53*, 1053–1064, doi:10.1016/j.pss.2005.02.008.

Grassi, D., V. Formisano, F. Forget, C. Fiorenza, N. I. Ignatiev, A. Maturilli, and L. V. Zasova (2007), The Martian atmosphere in the region of Hellas basin as observed by the planetary Fourier spectrometer (PFS-MEX), *Planet. Space Sci.*, *55*, 1346–1357, doi:10.1016/j.pss.2006.12.006.

Gray, L. D. (1966), Transmission of the atmosphere of Mars in the region of 2μ, *Icarus*, *5*, 390–398.

Haberle, R. M., and D. C. Catling (1996), A micro-meteorological mission for global network science on Mars: Rationale and measurement requirements, *Planet. Space Sci.*, *44*, 1361–1383.

Hess, S. L., J. A. Ryan, J. E. Tillman, R. M. Henry, and C. B. Leovy (1980), The annual cycle of pressure on Mars measured by Viking landers 1 and 2, *Geophys. Res. Lett.*, *7*, 197–200.

Hourdin, F., P. Le Van, F. Forget, and O. Talagrand (1993), Meteorological variability and the annual surface pressure cycle on Mars, *J. Atmos. Sci.*, *50*, 3625–3640.

Hourdin, F., F. Forget, and O. Talagrand (1995), The sensitivity of the Martian surface pressure to various parameters: A comparison between numerical simulations and Viking observations, *J. Geophys. Res.*, *100*, 5501–5523.

Houweling, S., W. Hartmann, I. Aben, H. Schrijver, J. Skidmore, G.-J. Roelofs, and F.-M. Breon (2005), Evidence of systematic errors in SCIAMACHY-observed CO_2 due to aerosols, *Atmos. Chem. Phys.*, *5*, 3003–3013.

Jacquinet-Husson, N., et al. (2005), The 2003 edition of the GEISA/IASI spectroscopic database, *J. Quant. Spectrosc. Radiat. Transfer*, *95*, 429–467.

Jouglet, D., F. Poulet, R. E. Milliken, J. F. Mustard, J.-P. Bibring, Y. Langevin, B. Gondet, and C. Gomez (2007), Hydration state of the Martian surface as seen by Mars Express OMEGA: 1. Analysis of the 3 μm hydration feature, *J. Geophys. Res.*, doi:10.1029/2006JE002846, in press.

Kanner, L. C., J. F. Mustard, and A. Gendrin (2007), Assessing the limits of the Modified Gaussian Model for remote spectroscopic studies of pyroxenes on Mars, *Icarus*, *187*, 442–456, doi:10.1016/j.icarus.2006.10.025.

Langevin, Y., J.-P. Bibring, F. Montmessin, F. Forget, M. Vincendon, S. Douté, F. Poulet, and B. Gondet (2007), Observations of the south seasonal cap of Mars during recession in 2004–2006 by the OMEGA visible/near-infrared imaging spectrometer on board Mars Express, *J. Geophys. Res.*, *112*, E08S12, doi:10.1029/2006JE002841.

Lewis, S. R., M. Collins, P. L. Read, F. Forget, F. Hourdin, R. Fournier, C. Hourdin, O. Talagrand, and J.-P. Huot (1999), A climate database for Mars, *J. Geophys. Res.*, *104*, 24,177–24,194.

Melchiorri, R., P. Drossart, T. Fouchet, B. Bézard, F. Forget, A. Gendrin, J. P. Bibring, N. Manaud, and Omega Team (2006), A simulation of the OMEGA/Mars Express observations: Analysis of the atmospheric contribution, *Planet. Space Sci.*, *54*, 774–783, doi:10.1016/j.pss.2006.04.014.

Mitchell, R. M., and D. M. O'Brien (1987), Error estimates for passive satellite measurement of surface pressure using absorption in the A band of oxygen, *J. Atmos. Sci.*, *44*, 1981–1990.

Montabone, L., S. R. Lewis, P. L. Read, and D. P. Hinson (2006), Validation of Martian meteorological data assimilation for MGS/TES using radio occultation measurements, *Icarus*, *185*, 113–132, doi:10.1016/j.icarus.2006.07.012.

Montmessin, F., E. Quémerais, J. L. Bertaux, O. Korablev, P. Rannou, and S. Lebonnois (2006), Stellar occultations at UV wavelengths by the SPICAM instrument: Retrieval and analysis of Martian haze profiles, *J. Geophys. Res.*, *111*, E09S09, doi:10.1029/2005JE002662.

Mustard, J. F., F. Poulet, A. Gendrin, J.-P. Bibring, Y. Langevin, B. Gondet, N. Mangold, G. Bellucci, and F. Altieri (2005), Olivine and pyroxene diversity in the crust of Mars, *Science*, *307*, 1594–1597, doi:10.1126/science.1109098.

Newman, C. E., S. R. Lewis, P. L. Read, and F. Forget (2002), Modeling the Martian dust cycle: 1. Representations of dust transport processes, *J. Geophys. Res.*, *107*(E12), 5123, doi:10.1029/2002JE001910.

O'Brien, D. M., R. M. Mitchell, S. A. English, and G. A. Da Costa (1997), Airborne measurements of air mass from O_2 A-band absorption spectra, *J. Atmos. Oceanic Technol.*, *15*, 1272–1286.

Ockert-Bell, M. E., J. F. Bell III., C. McKay, J. Pollack, and F. Forget (1997), Absorption and scattering properties of the Martian dust in the solar wavelengths, *J. Geophys. Res.*, *102*, 9039–9050.

Owen, T., K. Biemann, D. R. Rushneck, J. E. Biller, D. W. Howarth, and A. L. Lafleur (1977), The composition of the atmosphere at the surface of Mars, *J. Geophys. Res.*, *82*, 4635–4639.

Pleskot, L. K., and E. D. Miner (1981), Time variability of Martian bolometric albedo, *Icarus*, *45*, 179–201.

Press, W. H., S. A. Teukolsky, W. T. Vetterling, and B. P. Flannery (1992), *Numerical Recipes in FORTRAN: The Art of Scientific Computing*, Cambridge Univ. Press, Cambridge, U. K.

Rosenqvist, J. (1991), Mars: Etude de son atmosphère par le spectro-imageur ISM, Ph.D. thesis, Université Paris 7, Paris.

Rothman, L. S., et al. (2005), The HITRAN 2004 molecular spectroscopic database, *J. Quant. Spectrosc. Radiat. Transfer*, *96*, 139–204.

Schofield, J. T., D. Crisp, J. R. Barnes, R. M. Haberle, J. A. Magalhaães, J. R. Murphy, A. Seiff, S. Larsen, and G. Wilson (1997), The Mars Pathfinder Atmospheric Structure Investigation/Meteorology (ASI/MET) experiment, *Science*, *278*, 1752–1757.

Shkuratov, Y., M. Kreslavsky, V. Kaydash, G. Videen, J. Bell, M. Wolff, M. Hubbard, K. Noll, and A. Lubenow (2005), Hubble Space Telescope imaging polarimetry of Mars during the 2003 opposition, *Icarus*, *176*, 1–11, doi:10.1016/j.icarus.2005.01.009.

Smith, D. E., et al. (2001), Mars Orbiter Laser Altimeter: Experiment summary after the first year of global mapping of Mars, *J. Geophys. Res.*, *106*, 23,689–23,722.

Smith, M. D. (2004), Interannual variability in TES atmospheric observations of Mars during 1999–2003, *Icarus*, *167*, 148–165.

Smith, M. D. (2006), TES atmospheric temperature, aerosol optical depth, and water vapor observations 1999–2004, paper presented at Second Workshop on Mars Atmosphere Modelling and Observations, Cent. Natl. d'Etudes Spatiales, Granada, Spain.

Smith, M. D., J. C. Pearl, B. J. Conrath, and P. R. Christensen (2001), Thermal Emission Spectrometer results: Mars atmospheric thermal structure and aerosol distribution, *J. Geophys. Res.*, *106*(E10), 23,929–23,945.

Sobolev, V. V. (1975), *Light Scaterring in Planetary Atmospheres*, Pergamon, New York.

Spiga, A., F. Forget, B. Dolla, S. Vinatier, R. Melchiorri, P. Drossart, A. Gendrin, J.-P. Bibring, Y. Langevin, and B. Gondet (2007), Remote sensing of surface pressure on Mars with the Mars Express/OMEGA spectrometer: 2. Meteorological maps, *J. Geophys. Res.*, *112*, E08S16, doi:10.1029/2006JE002870.

Sprague, A. L., W. V. Boynton, K. E. Kerry, D. M. Janes, D. M. Hunten, K. J. Kim, R. C. Reedy, and A. E. Metzger (2004), Mars' south polar Ar enhancement: A tracer for south polar seasonal meridional mixing, *Science*, *306*, 1364–1367, doi:10.1126/science.1098496.

Stam, D. M., J. F. De Haan, J. W. Hovenier, and P. Stammes (1999), Degree of linear polarization of light emerging from the cloudless atmosphere in the oxygen A band, *J. Geophys. Res.*, *104*, 16,843–16,858.

Stam, D. M., J. F. De Haan, J. W. Hovenier, and I. Aben (2000), Detecting radiances in the O_2 A band using polarization-sensitive satellite instruments with application to the Global Ozone Monitoring Experiment, *J. Geophys. Res.*, *105*, 22,379–22,392.

Sunshine, J. M., C. M. Pieters, and S. F. Pratt (1990), Deconvolution of mineral absorption bands: An improved approach, *J. Geophys. Res.*, *95*, 6955–6966.

Tillman, J. E. (1988), Mars global atmospheric oscillations: Annually synchronized transient normal-mode oscillations and the triggering of global dust storms, *J. Geophys. Res.*, *93*(D8), 9433–9451.

Toth, R. A., L. R. Brown, C. E. Miller, V. M. Devi, and D. C. Benner (2006), Line strengths of $^{12}C^{16}O_2$: 4550–7000 cm^{-1}, *J. Mol. Spectrosc.*, *239*, 221–242, doi:10.1016/j.jms.2006.08.001.

Wolff, M. J., et al. (2006), Constraints on dust aerosols from the Mars Exploration Rovers using MGS overflights and Mini-TES, *J. Geophys. Res.*, *111*, E12S17, doi:10.1029/2006JE002786.

Zasova, L., et al. (2005), Water clouds and dust aerosols observations with PFS MEX at Mars, *Planet. Space Sci.*, *53*, 1065–1077, doi:10.1016/j.pss.2004.12.010.

Zurek, R. W., J. R. Barnes, R. M. Haberle, J. B. Pollack, J. E. Tillman, and C. B. Leovy (1992), Dynamics of the atmosphere of Mars, in *Mars*, edited by H. H. Kieffer, pp. 835–933, Univ. of Ariz. Press, Tucson.

J.-P. Bibring, A. Gendrin, B. Gondet, and Y. Langevin, Institut d'Astrophysique Spatiale, CNRS/Universit Paris Sud, Bâtiment 121, F-91405 Orsay, France.

B. Dolla, F. Forget, and A. Spiga, Laboratoire de Météorologie Dynamique, CNRS-UPMC BP99, 4 Place Jussieu, F-75252 Paris Cedex 05, France. (forget@lmd.jussieu.fr)

P. Drossart, R. Melchiorri, and S. Vinatier, LESIA, Observatoire de Paris-Meudon, 5 Place Jules Janssen, F-92195 Meudon Cedex, France.